Three-Dimensional Solution Structure of Oryzacystatin-I, a Cysteine Proteinase Inhibitor of the Rice, *Oryza sativa* L. japonica[†,‡]

Koji Nagata,[§] Norio Kudo,[§] Keiko Abe,[||] Soichi Arai,[||] and Masaru Tanokura*[,§,||]

Biotechnology Research Center and Department of Applied Biological Chemistry, The University of Tokyo, 1-1-1 Yayoi, Bunkyo-ku, Tokyo 113-8657, Japan

Received March 28, 2000; Revised Manuscript Received August 3, 2000

ABSTRACT: The three-dimensional structure of oryzacystatin-I, a cysteine proteinase inhibitor of the rice, *Oryza sativa* L. japonica, has been determined in solution at pH 6.8 and 25 °C by ^{1}H and ^{15}N NMR spectroscopy. The main body (Glu13−Asp97) of oryzacystatin-I is well-defined and consists of an α-helix and a five-stranded antiparallel β-sheet, while the N- and C-terminal regions (Ser2−Val12 and Ala98−Ala102) are less defined. The helix-sheet architechture of oryzacystatin-I is stabilized by a hydrophobic cluster formed between the α-helix and the β-sheet and is considerably similar to that of monellin, a sweet-tasting protein from an African berry, as well as those of the animal cystatins studied, e.g., chicken egg white cystatin and human stefins A and B (also referred to as human cystatins A and B). Detailed structural comparison indicates that oryzacystatin-I is more similar to chicken cystatin, which belongs to the type-2 animal cystatins, than to human stefins A and B, which belong to the type-1 animal cystatins, despite different loop length.

Cysteine proteinase inhibitors are widely distributed in mammals, plants, and insects and may function to protect cells from unwanted proteolysis and to control intra- and extracellular protein breakdown. The cystatin superfamily consists of tightly and reversibly binding inhibitors against cysteine proteinases of the papain family. The cystatin superfamily in higher animals can be divided into three types based on the molecular mass and the presence of disulfide bonds (*1*−*3*). Type 1 animal cystatins have ca. 100 amino acids, lack disulfide bonds, and are present predominantly intracellularly. Type 2 animal cystatins have ca. 120 amino acids, contain at least two characteristic disulfide bonds, and are found extracellularly, in body fluids. Type 3 animal cystatins are larger glycoproteins containing several type 2-like cystatin domains.

The cysteine proteinase inhibitors from plants that show amino acid sequence similarity to the animal cystatins are referred to as the phytocystatins (*4*). Oryzacystatin is the first well-defined phytocystatin (*4*−*9*). It occurs in the endosperm of the rice *Oryza sativa* L. japonica and has potent inhibitory activity against papain (EC 3.4.22.2) and several other cysteine proteinases. It is similar to the type 1 animal cystatins in that it consists of 102 amino acids and lacks disulfide bonds.

Thus far, the crystal structures of human stefin B (also referred to as cystatin B) complexed with carboxymethylated papain (CM[1]-papain) (*10*) and chicken egg white cystatin (*11*) and the solution structures of human stefin A (also referred to as cystatin A) (*12*, *13*) and chicken egg white cystatin (*14*) have been reported. These structures have shown that the types 1 and 2 animal cystatins studied share a common fold consisting of a five-stranded antiparallel β-sheet that wraps around a central α-helix. In the crystal structure of human stefin B−CM-papain complex, a wedge-shaped edge of human stefin B, formed by the two tight β-hairpin loops and the N-terminal region, slots into the active-site cleft of papain to achieve the tight binding (*10*). The first binding loop (L1) contains the highly conserved Gln−Xaa−Val−Xaa−Gly motif (Xaa represents any amino acid), the second binding loop (L2) contains an aromatic residue, Trp or His, and the third contact point, referred to as the N-terminal trunk (NT), contains a conserved Gly residue (*3*). Because all of the three structural motifs are present in oryzacystatin-I, it would inhibit papain in a similar manner. In fact, the mutation in L1 and the deletion of L2 both lead to significant loss in the papain-inhibitory activity of oryzacystatin-I (*15*), but the NT seems to be of relatively low importance for papain inhibition by oryzacystatin-I (*16*, *17*).

[†] This work was partly supported by Grants-in-Aid for Scientific Research from the Ministry of Education, Science, Sports and Culture of Japan.

[‡] The chemical shifts and the atomic coordinates have been deposited in BioMagResBank (code 4748) and Protein Data Bank (code 1EQK), respectively.

* To whom correspondence should be addressed. Telephone: +81-3-5841-5165. Fax: +81-3-5841-8023. E-mail: amtanok@mail.ecc.u-tokyo.ac.jp.

[§] Biotechnology Research Center.

[||] Department of Applied Biological Chemistry.

[1] Abbreviations: 2D, two-dimensional; 3D, three-dimensional; CM, carboxymethyl; DQF-COSY, double-quantum-filtered correlated spectroscopy; HSQC, heteronuclear single quantum-coherence; L1, first binding β-hairpin loop; L2, second binding β-hairpin loop; MALDI-TOF-MS, matrix-assisted laser desorption ionization time-of-flight mass spectrometry; NMR, nuclear magnetic resonance; NOE, nuclear Overhauser effect; NOESY, nuclear Overhauser effect spectroscopy; NT, N-terminal trunk; PDB, Protein Data Bank; RMS, root-mean-square; T_1, longitudinal relaxation time; T_2, transverse relaxation time; TOCSY, total correlated spectroscopy.

10.1021/bi0006971 CCC: $19.00
Published on Web 11/08/2000

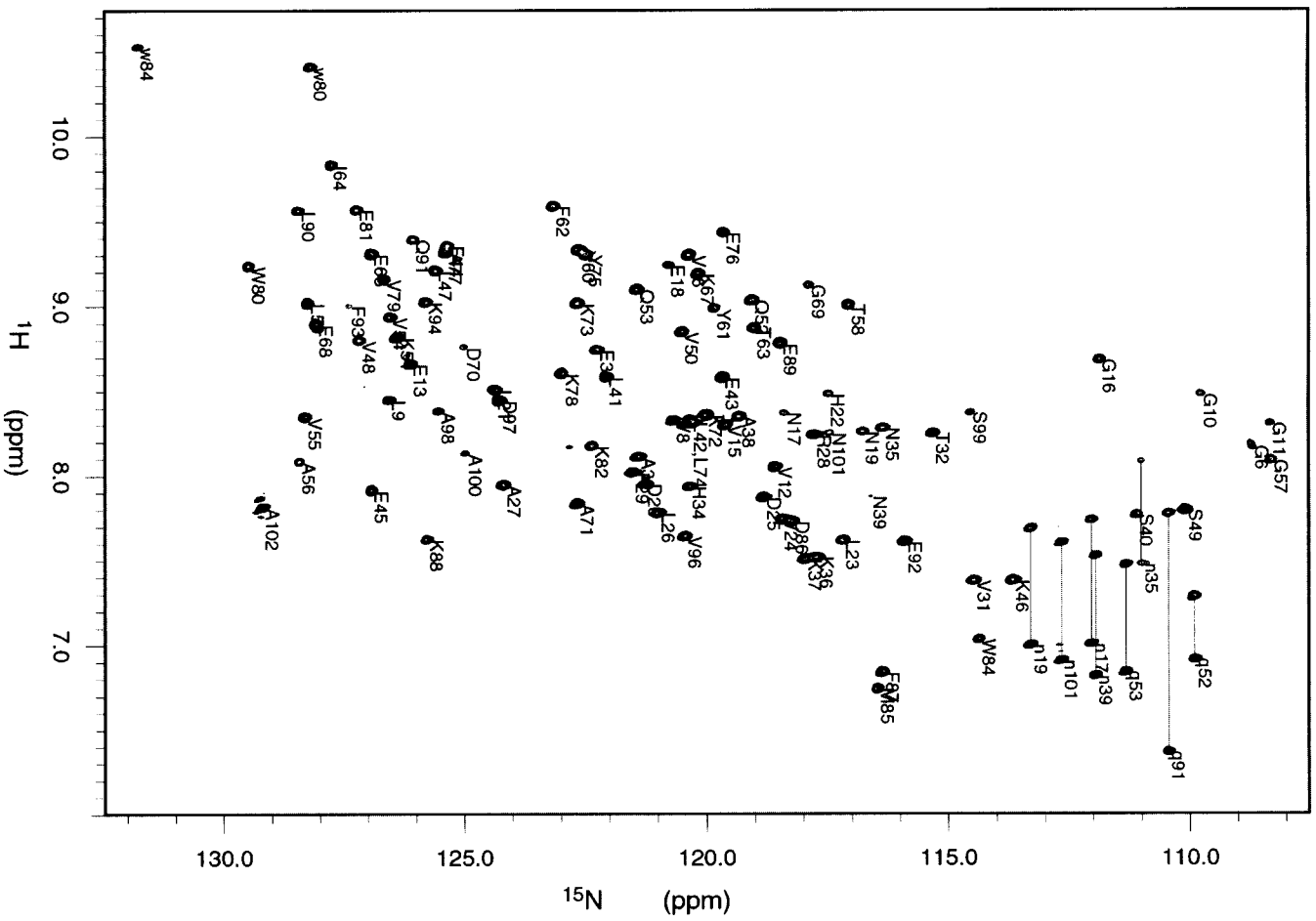

FIGURE 1: ^{1}H-^{15}N HSQC spectrum of uniformly ^{15}N-labeled oryzacystatin-I. The capital letters indicate the assignments for the backbone ^{1}H-^{15}N groups, while the small letters indicate the assignments for the side chain ^{1}H-^{15}N groups.

To investigate the molecular mechanisms of cysteine proteinase inhibition by oryzacystatin-I, we have determined its solution structure at pH 6.8 and 25 °C by ^{1}H and ^{15}N NMR spectroscopy and compared the structure with those of animal cystatins.

EXPERIMENTAL PROCEDURES

Sample Preparation. Recombinant oryzacystatin-I was overproduced by use of the expression vector pET-26b(+) and the host *Escherichia coli* BL21(DE3) (*18*). M9 minimal media containing ^{15}N-labeled NH_4Cl (99.4% ^{15}N; Shokotsusho, Tokyo) were used for the production of ^{15}N-labeled oryzacystatin-I. The oryzacystatin-I produced in *E. coli* was purified from the cell extract by ammonium sulfate fractionation followed by hydrophobic, anion exchange and size exclusion chromatographies with RESOURCE PHE, RESOURCE Q, and Superdex 75 columns (Pharmacia). MALDI-TOF-MS analysis showed that the heterologously produced oryzacystatin-I lacked the N-terminal Met and consisted of 101 amino acid residues. The purified oryzacystatin-I was concentrated with Centrisart ultracentrifugation tubes (Sartorius). The sample for NMR measurements contained 2−3 mM oryzacystatin-I dissolved in 50 mM sodium phosphate/100 mM NaCl/0.02% NaN_3, pH 6.8, in 10% ^2H_2O/90% H_2O.

NMR Spectroscopy. NMR data were collected at 25 °C on a Unity Inova 500-MHz spectrometer (Varian) equipped with a triple resonance probe with *z*-axis pulsed field gradients (Varian, Nalorac). Quadrature detection in the indirect dimensions of homonuclear and heteronuclear spectra was achieved using States (*19*) and States-TPPI (*20*), respectively. DQF-COSY (*21*), TOCSY (mixing time, 45 ms) (*22*), and NOESY (mixing time, 150 or 75 ms) (*23*) spectra of unlabeled oryzacystatin-I were recorded with a time-domain data size of 512 × 1024 complex points, $t_1$max (^{1}H) 73.1 ms, $t_2$max (^{1}H) 146.7 ms. In the homonuclear NMR measurements, the water resonance was suppressed by presaturation (*24*). ^{1}H-^{15}N HSQC (*25, 26*), ^{1}H-^{1}H-^{15}N TOCSY-HSQC (mixing time, 49 or 33 ms) (*27*), NOESY-HSQC (mixing time, 150 or 75 ms) (*28*), HNHA (*29*), ^{15}N T_1, ^{15}N T_2, and ^{15}N{^{1}H}-NOE (^{1}H saturation time, 3 s) (*30*) spectra of ^{15}N-labeled oryzacystatin-I were measured with pulse sequences using sensitivity enhancement and gradient selection (*26*). The heteronuclear 2D spectra were recorded with a time-domain size of 64 × 352 complex points, $t_1$max (^{15}N) 35.6 ms, $t_2$max (^{1}H) 50.4 ms. The heteronuclear 3D spectra were recorded with the time-domain size of 128 × 32 × 352 complex points, $t_1$max (^{1}H) 23.3 ms, $t_2$max (^{15}N) 17.8 ms, $t_3$max (^{1}H) 50.4 ms. The acquired NMR data were processed, visualized, and peak-picked with the softwares, NMRPipe (ver. 1.6) (*31*), NMRDraw (ver. 1.6) (*31*)/FELIX 97 (Molecular Simulations), and PIPP/CAPP (ver. 4.0) (*32*), respectively, on an Octane workstation (Silicon Graphics). Determination of ^{15}N T_1 and T_2 and estimation of the overall rotational correlation time were done as described (*30*).

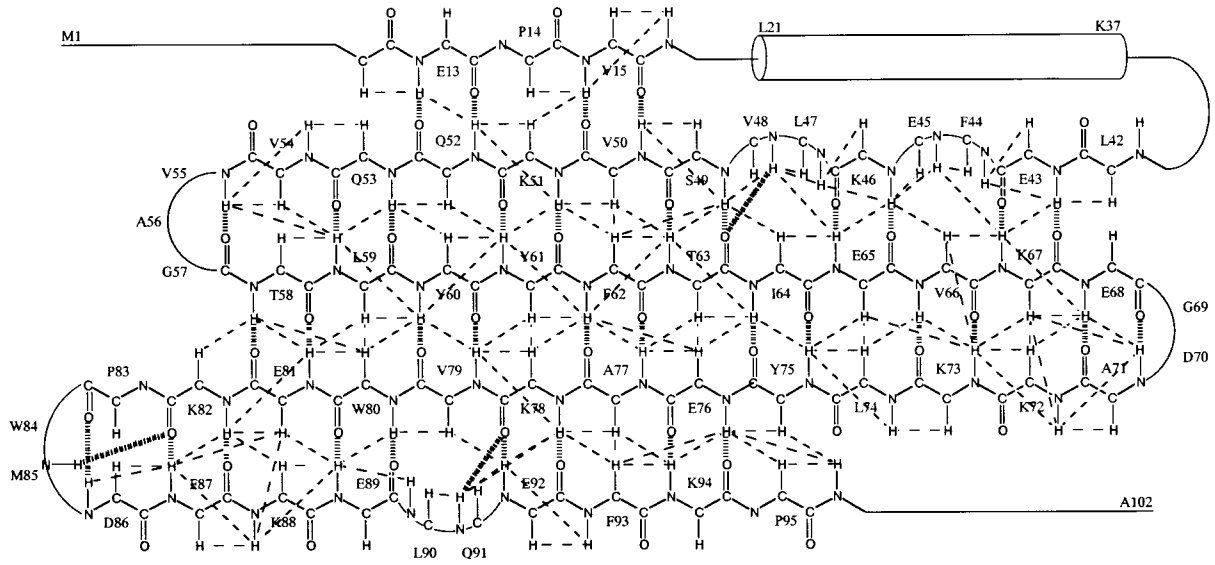

FIGURE 2: Diagram of antiparallel β-sheet regions in oryzacystatin-I. Interresidual NOEs between backbone protons (- - -) and hydrogen bonds (| | | | |) are shown.

NOE-Derived Interproton Distance Restraints. Interproton distance restraints were obtained from cross-peak intensities in the 3D ^{1}H-^{1}H-^{15}N NOESY-HSQC and 2D ^{1}H-^{1}H NOESY with a mixing time of 75 ms. The peak intensities were translated to interproton distances based on the relation of NOE $\propto$ (distance)$^{-6}$ and the standard distance between H^N_i and H^N_{i+1} in α-helix = 2.8 Å (*33*). Upper bound distance restraints were set to the calculated distances plus 0.5 Å considering internal mobility. Lower bound distance restraints were set to the sum of van der Waals radii. Pseudoatom corrections were added to the upper bound distance restraints involving degenerate protons from methylene groups and aromatic rings (*34*).

Torsion Angle Restraints. ϕ angle restraints were derived from $^3J_{HN-H\alpha}$ coupling constants obtained from 3D HNHA. ϕ angle was restrained to the range of $-160°$ to $-80°$ for $^3J_{HN-H\alpha} > 8$ Hz, $-140°$ to $-100°$ for $^3J_{HN-H\alpha} > 9$ Hz, and $-90°$ to $-40°$ for $^3J_{HN-H\alpha} < 6$ Hz. Stereospecific assignments of β-methylene protons and χ_1 angle restraints were derived from semiquantitative estimates of $^3J_{H\alpha-H\beta}$ obtained from 3D ^{1}H-^{1}H-^{15}N TOCSY-HSQC (33 ms mixing time) (*35*), NOE intensities between H^N and H^β obtained from a 3D ^{1}H-^{1}H-^{15}H NOESY-HSQC (75 ms mixing time) and NOE intensities between H^α and H^β obtained from 2D ^{1}H-^{1}H NOESY (75 ms mixing time). The ranges employed for χ_1 angle restraints were $60 \pm 50°$, $180 \pm 50°$, and $-60 \pm 50°$.

Hydrogen-Bond Distance Restraints. Hydrogen bonds were assigned between slowly exchanging amide protons and their respective carbonyl acceptors deduced from the NOE data with reference to the hydrogen bonds in the structures of other cystatin members (*10, 14*) and were explicitly defined as two distance restraints between the donor and the acceptor: $r_{HN-O} = 1.8-2.4$ Å and $r_{N-O} = 2.7-3.5$ Å. The exchange rate of amide protons was estimated from the difference in intensity of ^{1}H-^{15}N HSQC cross-peaks in spectra recorded with and without water presaturation (*36*).

Structure Calculations. Structure calculations were performed with the NMR-derived restraints including interproton distance restraints, hydrogen bond distance restraints, and torsion angle restraints (ϕ and χ_1). One hundred random conformers were annealed in 10 000 steps by torsion angle dynamics with the program DYANA (ver. 1.4) (*37*). Twenty conformers with the lowest DYANA target functions were used to represent the solution conformation of oryzacystatin-I. The average coordinate of the 20 DYANA conformers was subjected to energy minimization with the acceptavecalc module in CNS (ver. 0.9) (*38*).

Structure Analysis. Numerical analysis of the calculated structures was performed with the programs, DYANA (ver. 1.4) (*37*), CNS (ver. 0.9) (*38*), AQUA (ver. 2.0)/PROCHECK-NMR (ver. 3.4) (*39*), and MOLMOL (ver. 2.6) (*40*). Ramachandran $\phi-\psi$ plot analysis was done with PROCHECK-NMR (ver. 3.4) (*39*). Secondary structure was defined and tertiary structure was visualized with MOLMOL (ver. 2.6) (*40*). A residue was determined to be in a particular regular secondary-structure motif if it was found in that conformation in more than half of the 20 DYANA conformers.

RESULTS

Resonance Assignments. Spin system assignments were made with correlated cross-peaks on 2D ^{1}H-^{1}H DQF-COSY (*21*), TOCSY (50 ms mixing time) (*22*), and 3D ^{1}H-^{1}H-^{15}N TOCSY-HSQC (49 ms mixing time) (*27*) spectra. Sequence-specific resonance assignments were almost completed by following NOE connectivities between H^α_i and H^N_{i+1}, between H^β_i and H^N_{i+1} and between H^N_i and H^N_{i+1} on 2D ^{1}H-^{1}H NOESY (75 ms and 150 ms mixing time) (*23*) and 3D ^{1}H-^{1}H-^{15}N NOESY-HSQC (75 ms and 150 ms mixing time) (*28*) spectra. Aromatic spin systems were connected to intraresidual β-protons using 2D ^{1}H-^{1}H NOESY (75 and 150 ms mixing time). Figure 1 shows the ^{1}H-^{15}N HSQC spectrum of ^{15}N-labeled oryzacystatin-I. The cross-peaks are labeled with the assignments.

Secondary Structure. Figure 2 summarizes the backbone NOE connectivities, along with the hydrogen bonds deduced from the locations of slowly exchanging amide protons, in

[2] The numbering of amino acid residues in this article is based on the oryzacystatin-I homology numbering system shown in Figure 6.

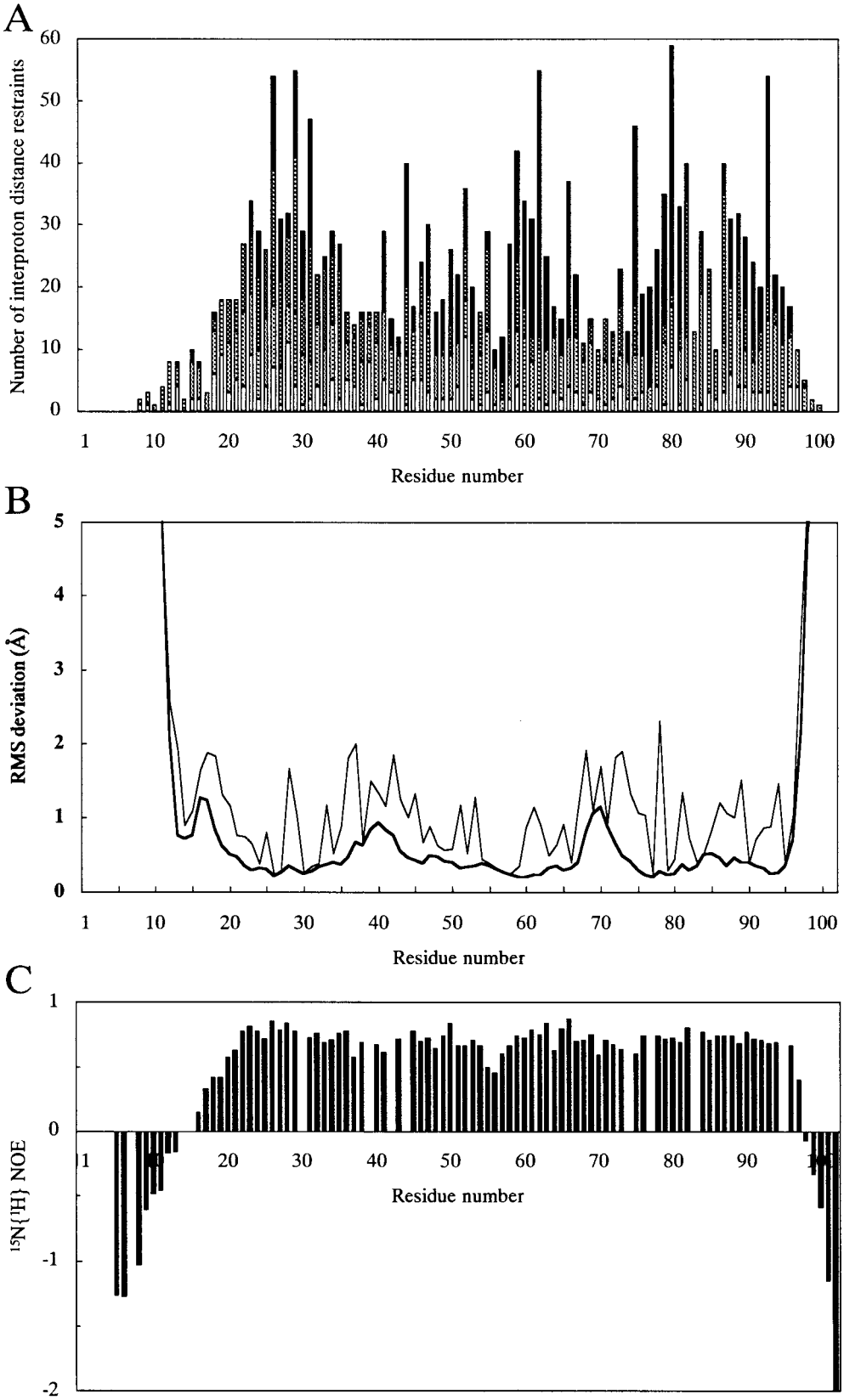

FIGURE 3: (A) Number of the NOE-derived interproton distance restraints for each residue. Intraresidual ($|i - j| = 0$), sequential ($|i - j| = 1$), medium-range ($2 \leq |i - j| \leq 5$), and long-range ($|i - j| \geq 6$) distance restraints are shown in white, light gray, dark gray, and black, respectively. (B) Atomic RMS deviation for each residue among the 20 structures. The heavy trace shows RMS deviation for the backbone atoms (N, C^{α}, and C′), while the thinner trace for the side chain non-hydrogen atoms. (C) ^{15}N{^{1}H}-NOE for each residue.

oryzacystatin-I. The data indicate that oryzacystatin-I consists of an α-helix (Leu21[2]−Lys37) and a five-stranded antiparallel β-sheet (the five β-strands are referred to as β1−β5, β1: Glu13−Val15, β2: Leu42−Val54, β3: Thr58−Glu68, β4: Lys73−Lys82 and β5: Phe87−Lys94). Three β-bulges, identified by weak NOE between H^{α}_{i} and H^{N}_{i+1} and strong

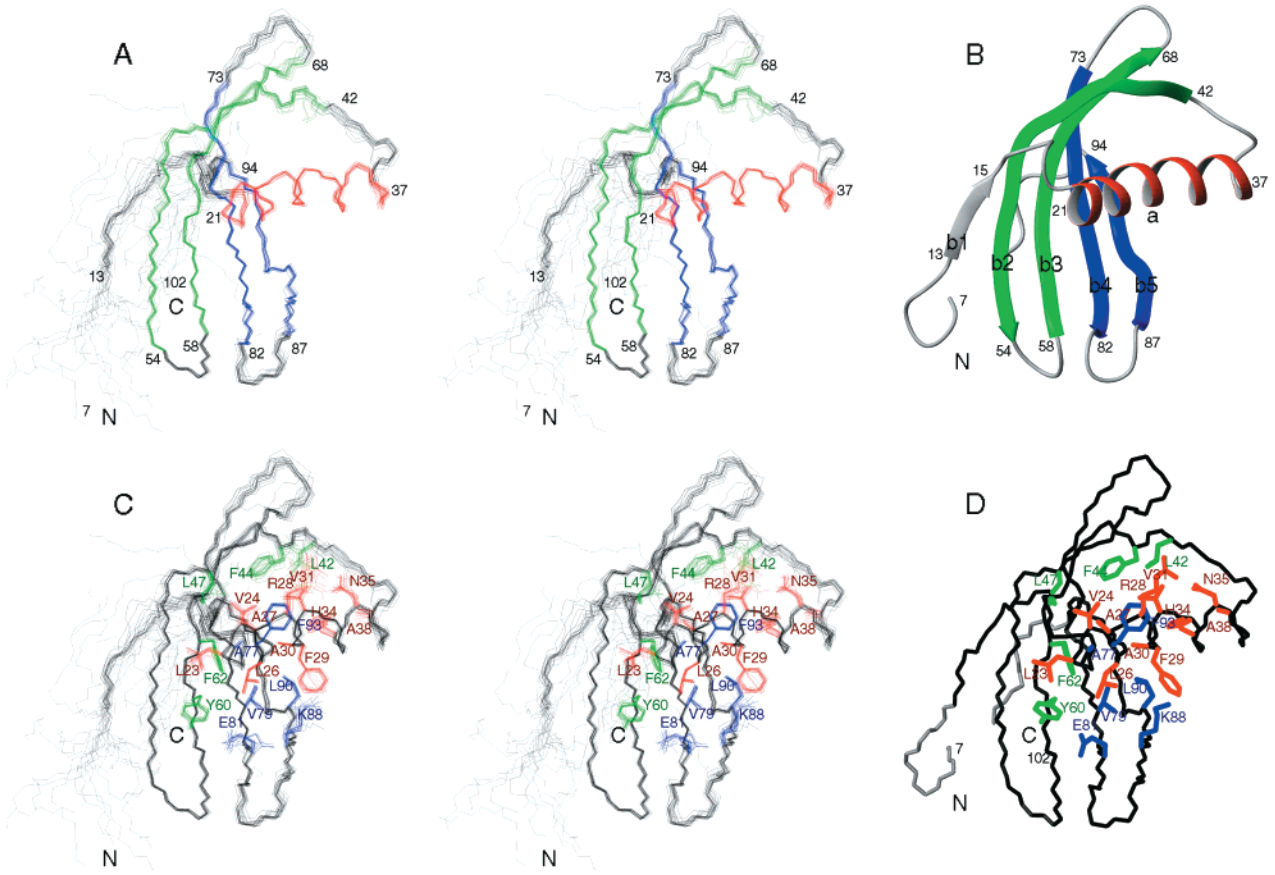

FIGURE 4: Stereopairs of the best-fit superposition of the 20 structures of oryzacystatin-I. (A) Backbone atoms (N, C^{α}, and C′). The main body (Glu13−Asp97) is shown in black, while the less defined N- and C-terminal regions (Pro7−Val12 and Ala98−Ala102) are in gray. The N-terminus without any defined conformation (Met1−Gly6) is not displayed. (B) Side chain non-hydrogen atoms involved in the interface of the α-helix and the β-sheet. The side chain atoms on the α-helix, antiparallel β-strands β2−β3 and β4−β5 are colored red, green, and blue, respectively, while the backbone atoms of the average structure are shown in black and gray as in panel A. Figure prepared with MOLMOL (*40*).

NOE between H^{N}_{i} and H^{N}_{i+1}, are found in β2 (Phe44−Glu45, Leu47−Val48), and β5 (Leu90−Gln91).

Structure Calculations. A total of 1383 experimentally derived restraints, consisting of 1183 interproton distance restraints (338 long-range ($|i - j| \geq 6$), 228 medium-range ($2 \leq |i - j| \leq 5$), 351 sequential ($|i - j| = 1$) and 266 intraresidual ($|i - j| = 0$)), 108 hydrogen bond restraints (representing 54 hydrogen bonds) (Figure S-1, see Supporting Information), and 92 torsion angle restraints (54 ϕ and 38 χ_1), were obtained and used in the structure calculations by simulated annealing in torsion angle space by use of DYANA (ver. 1.4) (*37*). A final set of 20 structures was selected from 100 calculations on the basis of agreement with the experimental data and van der Waals' energy. The average coordinates of the 20 DYANA structures were subjected to energy minimization in Cartesian space with CNS (ver. 0.9) (*38*). Table S-1 summarizes the structural statistics for the 20 structures and the energy-minimized average structure of oryzacystatin-I. All the structures satisfy the experimental restraints. There are no violations in interproton distances and torsion angles greater than 0.5 Å and 2°, respectively, in these structures. The solution conformation of oryzacystatin-I is well-defined except for the N- and C-terminal regions (Ser2−Val12 and Ala98−Ala102). The pairwise atomic RMS deviations among the 20 structures is 0.65 ± 0.17 Å for the backbone heavy atoms (N, C^{α}, C′) and 1.31 ± 0.16 Å for all non-hydrogen atoms in the well-defined region (Glu13−Asp97). Figure S-2 is the Ramachandran $\phi-\psi$ plot for the well-defined region of the energy-minimized structure, in which ca. 97% of the $\phi-\psi$ pairs are located in the allowed regions.

Figure 3 shows the number of the NOE-derived interproton distance restraints, the atomic RMS deviation, and the $^{15}N\{^{1}H\}$-NOE, respectively, for each residue. Although a large number of distance restraints were obtained for the main body of the molecule (Glu13−Asp97), only a few restraints were obtained for the N-terminal (Ser2−Gly11) and C-terminal (Ala98−Ala102) regions. As a result, the conformations of the N- and C-terminal parts are less defined. The scarce $^{1}H\{^{1}H\}$-NOEs, negative $^{15}N\{^{1}H\}$-NOEs and less defined conformations in the terminal regions all correlate with mobility faster than the overall rotational correlation time of the molecule, which is estimated to be 7.9 ± 0.2 ns from the T_1/T_2 ratio (*30*) of the residues in regular secondary structures except the highly mobile β1 (see Figure S-3).

Tertiary Structure. Figure 4, panel A shows the best-fit superposition of the backbone atoms and non-hydrogen atoms of oryzacystatin-I. The oryzacystatin-I molecule consists of a central α-helix (Leu21−Lys37) and a five-stranded antiparallel β-sheet (β1: Glu13−Val15, β2: Leu42−Val54, β3: Thr58−Glu68, β4: Lys73−Lys82, and β5: Phe87−Lys94). The α-helix runs roughly perpendicular to the direction of the β-strands. The β-sheet is somewhat

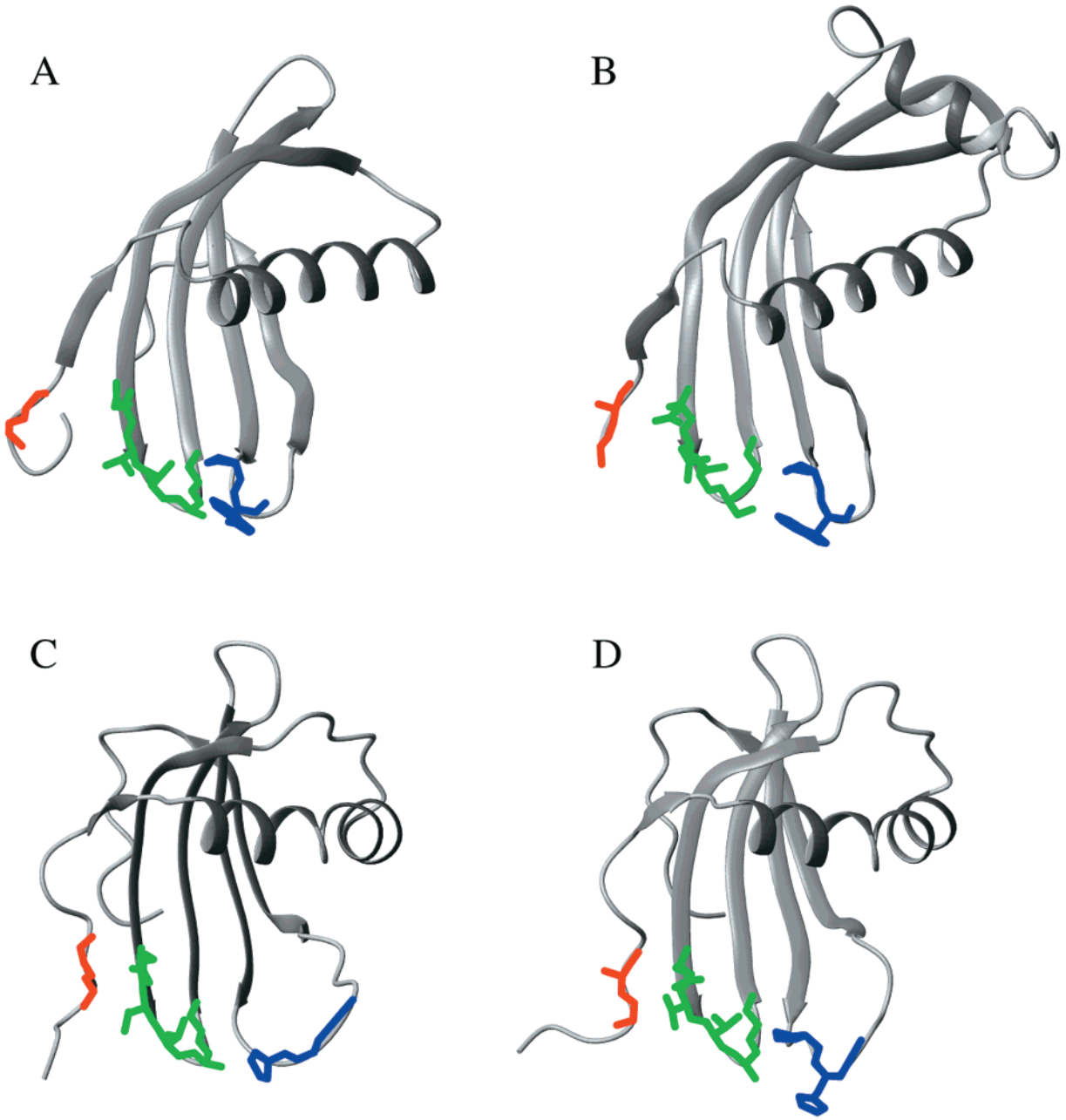

FIGURE 5: Structural comparison between oryzacystatin-I and animal cystatins: (A) oryzacystatin-I (solution structure), (B) chicken egg white cystatin (crystal structure, 1CEW), (C) human stefin A (solution structure, 1DVC), and (D) human stefin B (crystal structure, complexed with CM-papain, 1STF). The protein backbone is represented as ribbon. The backbone and side-chain non-hydrogen atoms of the amino acid residues involved in the N-terminal trunk (Gly10−Gly11, in the case of oryzacystatin-I), the first binding β-hairpin loop (Gln53−Val54−Val55−Ala56−Gly57), and the second binding β-hairpin loop (Pro83−Trp84) are shown in red, green, and blue, respectively. The second α-helix in chicken cystatin is an artifact of crystallization (*47*). Figure prepared with MOLMOL (*40*).

coiled. The coiling of the inner β-strands (β3 and β4) is smooth, but that of the edge strands (β2 and β5) are modified by the β-bulges (Phe44−Glu45 and Leu47−Val48 on β2 and Leu90−Gln91 on β5), that allows them to wrap around the α-helix. The primary core of oryzacystatin-I comprises a hydrophobic cluster in the interface between the α-helix and the β-sheet (Figure 4, panel B). The residues that contribute to this interface are Leu23, Val24, Leu26, Ala27, Arg28, Phe29, Ala30, Val31, His34, Asn35, Ala38 on the α-helix and Leu42, Phe44, Leu47 (on β2), Tyr60, Phe62 (on β3), Ala77, Val79, Glu81 (on β4), Lys88, Leu90, and Phe93 (on β5). Since the $^{15}N\{^1H\}$-NOEs in β1 are nearly zero and the interstrand $^1H\{^1H\}$-NOEs between β1 and β2 are weaker than those observed in the regular antiparallel β-sheet, the short N-terminal β-strand (β1: Glu13−Val15) is highly mobile and only weakly attached to β2.

DISCUSSION

The helix-sheet architecture of oryzacystatin-I is similar to those of the animal cystatins whose structures were solved, human stefin A (also referred to as cystatin A) (*12*, *13*), human stefin B (also referred to as cystatin B) (*10*), and chicken egg white cystatin (*11*, *14*) (Figure 5) and, in addition, to that of monellin, a sweet-tasting protein from the West African berry *Dioscoreophyllum cumminsii* (*41*−*43*) as predicted by Murzin (*44*) based on the 23% amino acid sequence identity. Table 1 shows the scores of conformational similarity between oryzacystatin-I and other mem-

FIGURE 6: Amino acid sequence alignment of oryzacystatin-I and related molecules based on the conformational similarity obtained from the DALI server (*45*). OC-I, oryzacystatin-I; CEWC, chicken egg white cystatin; HS-A, human stefin A; HS-B, human stefin B; MO-A and -B, the A- and B-chains of monellin. The secondary structure and residue number are shown above and below the amino acid sequence of oryzacystatin-I. An array of at marks (@@@) indicates an α-helix, an arrow (==>) indicates a β-strand, and a hat (^) indicates a β-bulge. The proposed active-site residues in cystatins (the N-terminal trunk, first and second binding β-hairpin loops) are colored red, green, and blue, respectively, while those in monellin are colored magenta.

bers of the cystatin superfamily and monellin obtained from the DALI server (*45*). The solution structure of oryzacystatin-I is the most similar to the crystal structure of chicken egg white cystatin (PDB code, 1CEW) (*11*) and the crystal structure of monellin (1MOL) (*46*), then to the crystal structure of human stefin B (1STF) complexed with CM-papain (*10*), the solution structure of human stefin A (1DVC) (*12*), the solution structure of chicken egg white cystatin (1A67) (*14*) and the solution structure of human stefin A (1CYV) (*13*). Figure 6 is the amino acid sequence alignment based on the conformational similarity obtained from the DALI server (*45*). The differences in lengths of polypeptide chains are exclusively located in the terminal and loop regions, and thus these molecules can adopt the common architecture.

Detailed structural comparison shows that oryzacystatin-I is more similar to chicken egg white cystatin than to human stefins A and B, particularly in (a) the conformation and length of the second binding β-hairpin loop (L2, located between β4 and β5), (b) the position of the N-terminal β-strand (β1), and (c) the orientation of the central α-helix (Figure 5). The second binding loops (L2's) of oryzacystatin-I and chicken egg white cystatin are shorter than those of human stefins A and B by two residues, and as a result, the L2's of the former are narrower than those of the latter (Figure 5). The N-terminal β-strands (β1's) of oryzacystatin-I and chicken egg white cystatin begin at the position 13, while those of human stefins A and B at the position 16 (Figure 5). The central α-helices of oryzacystatin-I and chicken cystatin are somewhat bent or straight, while the α-helix of human stefins A and B are kinked into halves (Figure 5). Because none of the NOE-derived distance restraints in oryzacystatin-I indicate the presence of kink as seen in human stefins A and B, we have judged that the α-helix in oryzacystatin-I is not kinked, but we could not judge whether the α-helix in oryzacystatin-I is slightly bent or straight in solution.

Table 1: Structural Similarity between Oryzacystatin-I and Other Molecules

	Z-score[a]	RMSD (Å)[b]
chicken egg white cystatin (crystal, 1CEW)	10.1	2.4
human stefin B (crystal, 1STF)[c]	7.9	2.4
human stefin A (solution, 1DVC)	7.9	2.9
chicken egg white cystatin (solution, 1A67)	4.6	3.2
human stefin A (solution, 1CYV)	1.7	3.3
monellin (crystal, 1MOL)	9.7	2.3

[a] Z-score shows the strength of similarity in three-dimensional structure in standard deviations above expected. [b] RMSD shows the positional RMS deviation of superimposed C^{α} atoms. [c] Crystal structure of human stefin B complexed with CM-papain.

ACKNOWLEDGMENT

We thank Drs. S. Tate (Japan Advanced Institute of Science and Technology), H. Kaji (Tokyo Metropolitan University), N. Nemoto (Varian Japan), T. Saito (LA Systems), F. Delaglio, and D. Garrett (National Institutes of Health), for valuable discussion and advice, and the Toronto NMR group of Dr. L. E. Kay for Varian pulse sequences.

SUPPORTING INFORMATION AVAILABLE

Table showing the structural statistics for the 20 DYANA structures and the CNS minimized average structure of oryzacystatin-I and the figures including the diagonal plots showing the distance restraints and the distances in the minimized average structure between residue pairs, the Ramachandran $\phi-\psi$ plot and the plot of ^{15}N T_1 and T_2 for

each residue. These materials are available free of charge via the Internet at http://pubs.acs.org.

REFERENCES

1. Barrett, A. J. (1986) *Biomed. Biochim. Acta 45*, 1363−1374.
2. Rawlings, N. D., and Barrett, A. J. (1990) *J. Mol. Evol. 30*, 60−71.
3. Turk, V., and Bode, W. (1991) *FEBS Lett. 285*, 213−219.
4. Abe, K., Kondo, H., Watanabe, H., Emori, Y., and Arai, S. (1991) *Biomed. Biochim. Acta 50*, 637−641.
5. Abe, K., Emori, Y., Kondo, H., Suzuki, K., and Arai, S. (1987) *J. Biol. Chem. 262*, 16793−16797.
6. Kondo, H., Emori, Y., Abe, K., Suzuki, K., and Arai, S. (1989) *Gene 81*, 259−265.
7. Kondo, H., Abe, K., Nishimura, I., Watanabe, H., Emori, Y., and Arai, S. (1990) *J. Biol. Chem. 265*, 15832−15837.
8. Kondo, H., Abe, K., Emori, Y., and Arai, S. (1991) *FEBS Lett. 278*, 87−90.
9. Arai, S., Abe, K., and Emori, Y. (1996) *Adv. Exp. Med. Biol. 389*, 73−78.
10. Stubbs, M. T., Laber, B., Bode, W., Huber, R., Jerala, R., Lenarcic, B., and Turk, V. (1990) *EMBO J. 9*, 1939−1947.
11. Bode, W., Engh, R., Musil, D., Thiele, U., Huber, R., Karshikov, A., Brzin, J., Kos, J., and Turk, V. (1988) *EMBO J. 7*, 2593−2599.
12. Martin, J. R., Craven, C. J., Jerala, R., Kroon-Zitko, L., Zerovnik, E., Turk, V., and Waltho, J. P. (1995) *J. Mol. Biol. 246*, 331−343.
13. Tate, S., Ushioda, T., Utsunomiya-Tate, N., Shibuya, K., Ohyama, Y., Nakano, Y., Kaji, H., Inagaki, F., Samejima, T., and Kainosho, M. (1995) *Biochemistry 34*, 14637−14648.
14. Dieckmann, T., Mitschang, L., Hofmann, M., Kos, J., Turk, V., Auerswald, E. A., Jaenicke, R., and Oschkinat, H. (1993) *J. Mol. Biol. 234*, 1048−1059.
15. Arai, S., Watanabe, H., Kondo, H., Emori, Y., and Abe, K. (1991) *J. Biochem. 109*, 294−298.
16. Abe, K., Emori, Y., Kondo, H., Arai, S., and Suzuki, K. (1988) *J. Biol. Chem. 263*, 7655−7659.
17. Chen, M. S., Johnson, B., Wen, L., Muthukrishnan, S., Kramer, K. J., Morgan, T. D., and Reeck, G. R. (1992) *Protein Expr. Purif. 3*, 41−49.
18. Kudo, N., Nishiyama, M., Sasaki, H., Abe, K., Arai, S., and Tanokura, M. (1998) *J. Biochem. 123*, 568−570.
19. States, D. J., Haberkorn, R. A., and Ruben, D. J. (1982) *J. Magn. Reson. 48*, 286−292.
20. Marion, D., Ikura, M., Tschudin, R., and Bax, A. (1989) *J. Magn. Reson. 85*, 393−399.
21. Rance, M., Sørensen, O. W., Bodenhausen, G., Wagner, G., Ernst, R. R., and Wüthrich, K. (1983) *Biochem. Biophys. Res. Commun. 117*, 479−485.
22. Bax, A., and Davis, D. G. (1985) *J. Magn. Reson. 65*, 355−360.
23. Macura, S., Huang, Y., Suter, D., and Ernst, R. R. (1981) *J. Magn. Reson. 43*, 259−281.
24. Zuiderweg, E. R. P., Hallenga, K., and Olejniczak, E. T. (1986) *J. Magn. Reson. 70*, 336−343.
25. Bodenhausen, G., and Ruben, D. J. (1980) *Chem. Phys. Lett. 69*, 185−189.
26. Kay, L. E., Keifer, P., and Saarinen, T. (1992) *J. Am. Chem. Soc. 114*, 10663−10665.
27. Marion, D., Kay, L. E., Sparks, S. W., Torchia, D. A., and Bax, A. (1989) *J. Am. Chem. Soc. 111*, 1515−1517.
28. Marion, D., Driscoll, P. C., Kay, L. E., Wingfield, P. T., Bax, A., Gronenborn, A. M., and Clore, G. M. (1989) *Biochemistry 28*, 6150−6156.
29. Vuister, G. W., and Bax, A. (1993) *J. Am. Chem. Soc. 115*, 7772−7777.
30. Farrow, N. A., Muhandiram, R., Singer, A. U., Pascal, S. M., Kay, C. M., Gish, G., Shoelson, S. E., Pawson, T., Forman-Kay, J. D., and Kay, L. E. (1994) *Biochemistry 33*, 5984−6003.
31. Delaglio, F., Grzesiek, S., Vuister, G. W., Zhu, G., Pfeifer, J., and Bax, A. (1995) *J. Biomol. NMR 6*, 277−293.
32. Garrett, D. S., Powers, R., Gronenborn, A. M., and Clore, G. M. (1991) *J. Magn. Reson. 95*, 214−220.
33. Wüthrich, K. (1986) *NMR of Proteins and Nucleic Acids*, John Wiley & Sons, New York.
34. Wüthrich, K., Billeter, M., and Braun, W. (1983) *J. Mol. Biol. 169*, 949−961.
35. Clore, G. M., Bax, A., and Gronenborn, A. M. (1991) *J. Biomol. NMR 1*, 13−22.
36. Spera, S., Ikura, M., and Bax, A. (1991) *J. Biomol. NMR 1*, 155−165.
37. Güntert, P., Mumenthaler, C., and Wüthrich, K. (1997) *J. Mol. Biol. 273*, 283−298.
38. Brünger, A. T., Adams, P. D., Clore, G. M., DeLano, W. L., Gros, P., Grosse-Kunstleve, R. W., Jiang, J. S., Kuszewski, J., Nilges, M., Pannu, N. S., Read, R. J., Rice, L. M., Simonson, T., and Warren, G. L. (1998) *Acta Crystallogr. D54*, 905−921.
39. Laskowski, R. A., Rullmann, J. A., MacArthur, M. W., Kaptein, R., and Thornton, J. M. (1996) *J. Biomol. NMR 8*, 477−486.
40. Koradi, R., Billeter, M., and Wüthrich, K. (1996) *J. Mol. Graphics 14*, 51−55.
41. Morris, J. A., and Cagan, R. H. (1972) *Biochim. Biophys. Acta 261*, 114−122.
42. Morris, J. A., Martenson, R., Deibler, G., and Cagan, R. H. (1973) *J. Biol. Chem. 248*, 534−539.
43. Kohmura, M., Nio, N., and Ariyoshi, Y. (1990) *Agric. Biol. Chem. 54*, 2219−2224.
44. Murzin, A. G. (1993) *J. Mol. Biol. 230*, 689−694.
45. Holm, L., and Sander, C. (1993) *J. Mol. Biol. 233*, 123−138.
46. Somoza, J. R., Jiang, F., Tong, L., Kang, C. H., Cho, J. M., and Kim, S. H. (1993) *J. Mol. Biol. 234*, 390−404.
47. Engh, R. A., Dieckmann, T., Bode, W., Auerswald, E. A., Turk, V., Huber, R., and Oschkinat, H. (1993) *J. Mol. Biol.* 234, 1060−1069.

BI0006971